Journal of Solid State Chemistry 183 (2010) 2400–2405

Contents lists available at ScienceDirect

Journal of Solid State Chemistry

journal homepage: www.elsevier.com/locate/jssc

A primitive tetragonal intermediate in the orthorhombic–cubic phase transition of perovskite-type strontium niobate $Sr_{0.92}NbO_3$

René B. Macquart [a], Brendan J. Kennedy [a,*], Maxim Avdeev [b]

[a] School of Chemistry, The University of Sydney, Sydney, NSW 2006, Australia
[b] Bragg Institute, Australian Nuclear Science and Technology Organisation, Private Mail Bag 1, Menai, NSW 2234, Australia

ARTICLE INFO

Article history:
Received 26 February 2010
Received in revised form
21 July 2010
Accepted 1 August 2010
Available online 5 August 2010

Keywords:
Perovskite
Phase transition
Neutron diffraction
Mode analysis

ABSTRACT

The Sr deficient perovskite $Sr_{0.92}NbO_3$ was synthesized from $Sr_5Nb_4O_{15}$ and Nb and its crystal structure was determined using powder neutron diffraction. At room temperature the structure is orthorhombic in space group *Pnma* with both in-phase and out-of-phase tilting of the NbO_6 octahedra. High temperature measurements have shown that the oxide undergoes a sequence of phase transitions with increasing temperature: $Pnma \rightarrow P4/mbm \rightarrow Pm\bar{3}m$. The intermediate tetragonal phase has only in-phase tilts of the NbO_6 octahedra, rather than the out-of-phase tilts present in the more commonly observed $I4/mcm$ structure, due to initial softening at the *M* point rather than *R* point. The tetragonal phase exists only over a very narrow temperature range. The importance of *M*–*M* and *M*–O bonding in controlling the transition temperatures in $SrMO_3$ perovskites is discussed.

1. Introduction

The description of the ideal ABX_3 perovskite, where the larger *A*-type cations are surrounded by 12 anions (*X*, typically oxygen or a halide) in a cubic–octahedral coordination and the *B*-type cations are surrounded by six anions in an octahedral arrangement, belies the flexibility of the perovskite-type structure, which leads to the myriad of perovskites encountered in solid state chemistry. The, often subtle, structural distortions exhibited by perovskites can be critical in controlling the physical properties of a given perovskite system and numerous studies of structure–property relationships have now been reported.

Crystallographic phase transitions in perovskites have been of interest for many years, reflecting their importance in solid state chemistry and condensed matter physics, and also because of the significance of perovskite-like phases in earth sciences. For example $NaNbO_3$ reportedly forms seven different modifications, including at least one ferroelectric form, between 100 and 915 K. As evident from studies of $SrZrO_3$, establishing the precise sequence of phase transitions in perovskites can be complicated by pseudo-symmetry [1–3] and is best achieved using a combination of high resolution powder diffraction and fine temperature intervals. Using such an approach, Howard et al. [4] showed the sequence of structures in $SrZrO_3$ to be $Pnma \rightarrow Imma \rightarrow I4/mcm \rightarrow Pm\bar{3}m$ with increasing temperature. Subsequently this sequence was reported for $SrRuO_3$ [5] and $SrSnO_3$ [6]. In the case of $SrRhO_3$ [7] the sample decomposes before the cubic phase could be identified and for $SrMoO_3$ [8] the *Imma* phase persisted down to 5 K such that the *Pnma* phase could not be realised. It appears that the second row oxides $SrMO_3$ (*M*=Zr, Mo, Ru and Rh) together with $SrSnO_3$ all exhibit the same sequence of phases, even if experimentally all four phases have not been directly observed for each oxide. Little, however, is known for the remaining second row strontium perovskite, $SrNbO_3$.

Ridgey and Ward [9] were apparently the first to prepare $SrNbO_3$ in 1955 and they described this as a cubic perovskite with a=4.024 Å. Almost 50 years later Hannerz et al. [10], using a combination of neutron diffraction and transmission electron microscopy, concluded that $Sr_{1-x}NbO_3$ adopts an orthorhombic perovskite-like structure at room temperature that is described in space group *Pnma* with $a \approx c \approx \sqrt{2}a_p$ and $b \approx 2a_p$, where a_p is the cell parameter of the idealised cubic perovskite. This structure is characterised by displacement of the anions inducing tilting of the NbO_6 octahedra. At around the same time Peng et al. [11] described $Sr_{0.97}NbO_3$ as having an orthorhombic cell with $a \approx c \approx \sqrt{2}a_p$ and $b \approx 2a_p$ but in $P2_12_12_1$ as a consequence of tilting of the NbO_6 octahedra and the formation of an ordered array of distorted NbO_6 octahedra. Evidently the structure of "$SrNbO_3$" is dependent on the precise Sr:Nb ratio; indeed a simple cubic structure in $Pm\bar{3}m$ has been described for the Sr defect oxides $Sr_{1-x}NbO_3$, $0.05 \leq x \leq 0.25$ [12]. Doping $SrNbO_3$ with Na results in the formation of a tetragonal cell in $P4/mbm$ [13].

No temperature dependent structural studies of "$SrNbO_3$" have been reported, and as part of our on-going studies of phase transitions in perovskites [1,14–17] we sought to establish this. Here we describe high temperature neutron diffraction data that

* Corresponding author.
E-mail addresses: kennedyb@chem.usyd.edu.au, B.Kennedy@chem.usyd.edu.au (B.J. Kennedy).

0022-4596/$ - see front matter © 2010 Elsevier Inc. All rights reserved.
doi:10.1016/j.jssc.2010.08.001

show that unlike in $SrZrO_3$ and $SrMoO_3$, the phase transition sequence in "$SrNbO_3$" is $Pnma \rightarrow P4/mbm \rightarrow Pm\bar{3}m$. In $SrNbO_3$ the intermediate tetragonal phase exists over a small ($\sim$20 K) temperature range.

2. Experimental

$Sr_{0.92}NbO_3$ powder was obtained during the attempted synthesis of $SrNbO_3$ from stoichiometric amounts of $Sr_5Nb_4O_{15}$ and Nb (Alfa Aesar, 325 mesh, 99.8%) that were mixed with an agate mortar and pestle under acetone. Once dry the mixture was pressed (65 MPa) into a rod (5 mm diameter $\times$ 50 mm long) using a hydrostatic press and then dried in an oven at 110 °C for $\sim$3 h. The dry rod was placed in a seamless niobium tube (Refrachina, 99.9%, OD 12 mm $\times$ 10 mm ID) with one end previously sealed with a tig welder. The tube was then evacuated and crimped shut by folding the end over and hammering flat. The sealed tube was placed in an alumina boat and heated (5 h from room temperature to 1500 °C, 72 h at 1500 °C, then step cooled) in a tube furnace under flowing argon (BOC, 99.99%, $\sim$1 cm^3/s). The sample was ground and X-ray diffraction, with a PANalytical X'Pert PRO MPD, used to check for purity. When synthesized $Sr_{0.92}NbO_3$ has a dark red colour, which tends to go brownish when exposed to air. The sample was stored in an evacuated desiccator when not in use. The precursor, $Sr_5Nb_4O_{15}$, was made by mixing stoichiometric amounts of $SrCO_3$ (Aldrich, 99.5+%) and Nb_2O_5 (Aithaca, 99.998%) under acetone with an agate mortar and pestle, allowing the mixture to dry, placing it in an alumina crucible, heating it in air at a rate of 15 °C/h and regrinding between steps (1000 °C $-$15 h $\times$ 3, 1250 °C$-$48 h, 1300 °C$-$48 h, 1300 °C$-$24 h).

Neutron powder diffraction data of a polycrystalline sample of $Sr_{0.92}NbO_3$ were measured using the high resolution powder diffractometer Echidna at ANSTO's OPAL facility at Lucas Heights using a wavelength of 1.622 Å [18]. This instrument has a maximum resolution of $\Delta d/d \sim 1 \times 10^{-3}$, with data collection typically taking 4 h. For these measurements the sample was contained in a cylindrical vanadium can that was mounted in a closed cycle helium refrigerator. The synchrotron X-ray diffraction data were collected at ambient temperature in the angular range $5^\circ < 2\theta < 85^\circ$, using X-rays of wavelength 0.82706 Å on the powder diffractometer at BL-10 of the Australian Synchrotron [19]. The sample was housed in a 0.3 mm diameter capillary, which was rotated during the measurements. The structures were refined using the program RIETICA [20]. The neutron peak shape was modelled using a pseudo-Voigt function and the background was estimated by interpolating between up to 40 selected points. Anisotropic displacement parameters were refined, in the tetragonal and cubic phases, from the neutron diffraction data. Larger than typical ESDs for the positional parameters were obtained apparently as a consequence of the high pseudo-symmetry of the structure.

3. Results and discussion

X-ray diffraction profile for $Sr_{0.92}NbO_3$ recorded at room temperature confirmed the formation of an orthorhombic phase, and no traces of unreacted Nb metal or Nb sub-oxides were observed in the pattern. The structure of $Sr_{0.92}NbO_3$ between 25 and 790 K was investigated using neutron powder diffraction data. The profile showed a small number of weak peaks from an unidentified impurity. These peaks could not be indexed to any known strontium niobium oxide. In addition to the strong Bragg reflections characteristic of the perovskite structure the neutron profiles collected in the temperature range $25\,K \leq T \leq 360\,K$ revealed a number of reflections of the type $(1/2)(oeo)_p$, $h \neq l$ ("o" indicates a Miller index with an odd number and "e" with even number), indicative of the presence of in-phase tilting of the NbO_6 octahedra and of the type $(1/2)(ooo)_p$, from out-of-phase tilts. The former ones are identified using the Glazer notation with + superscripts and are associated with M point distortions whilst the out-of-phase or "$-$" tilts are associated with R point distortions.

These superlattice reflections can be used to establish the space group of the perovskite and demonstrate that the structure of $Sr_{0.92}NbO_3$ was orthorhombic in $Pnma$ with $a \approx c \approx \sqrt{2}a_p$ and $b \approx 2a_p$ as described by Hannerz et al. [10]. There was no evidence from the diffraction patterns to indicate that the structure was orthorhombic in $Cmcm$. We note that whereas the neutron profiles did not reveal any resolved splitting indicative of orthorhombic symmetry, the X-ray patterns did. Conversely the superlattice reflections evident in the neutron profiles were very weak in the X-ray patterns. Refinement of the structure in $Pnma$ against the neutron data proved satisfactory, and an example is given in Fig. 1. The same model provided a good fit to the synchrotron data (Fig. 2). The tilt system in $Pnma$ is $a^-b^+a^-$ corresponding to out-of-phase (negative) tilts about [1 0 1] and in-phase tilts (positive) abut [0 1 0]. Intriguingly the magnitudes

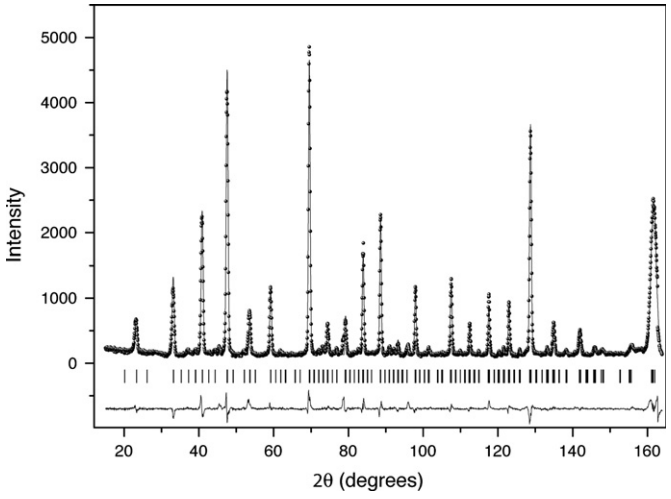

Fig. 1. Observed, calculated and difference neutron diffraction profiles for $Sr_{0.92}NbO_3$ recorded at room temperature with $\lambda = 1.622$ Å.

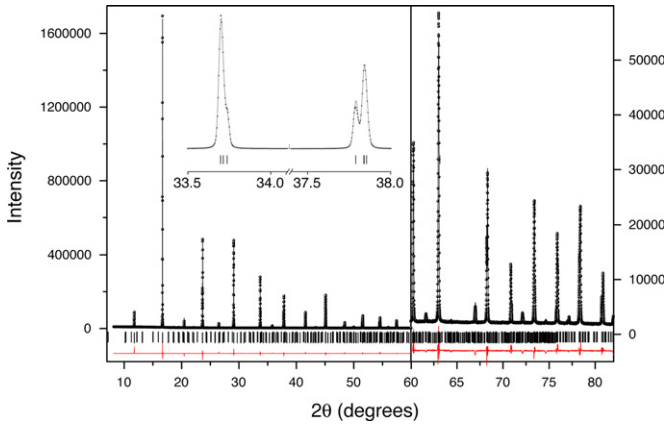

Fig. 2. Observed, calculated and difference synchrotron X-ray diffraction profiles for $Sr_{0.92}NbO_3$ recorded at room temperature with $\lambda = 0.82706$ Å. Note the change in intensity scale at 60°. The inset illustrates the resolved splitting of selected Bragg reflections.

of the two tilts estimated from the refined atomic coordinates [21] are very similar, 5.15° and 5.36°, at 25 K. Attempts to refine the structure at either 25 or 300 K using the model in $P2_12_12_1$ described by Peng et al. [11] were unsuccessful. Refinement of Sr occupancy against the synchrotron data suggests that the sample is Sr deficient, with a final stoichiometry of $Sr_{0.924(8)}NbO_3$.

The observed tilting of the octahedra in $Sr_{0.92}NbO_3$ is consistent with the tolerance factor, $t=(r_{Sr}+r_O)/(\sqrt{2}(r_{Nb}+r_O))=0.965$, calculated assuming the ionic radii for 6-coordinate Nb^{4+} is 0.68 Å, 12-coordinate Sr^{2+} is 1.44 Å and 6-coordinate O^{2-} is 1.40 Å [22], and reflects the need to optimise the bonding of both the Nb and Sr cations. The average Nb–O distance in $Sr_{0.92}NbO_3$ at room temperature is 2.02 Å, which is similar to the average Nb–O distance reported recently for $CaNbO_3$ [23], $BaNbO_3$ [24] and for the *Pnma* form of $SrNbO_3$ described by Hannerz et al. [10]. The bond valence sum for the Nb cation at room temperature is 4.13, as expected for a Nb^{4+} cation. Neglecting the effect of the Sr non-stoichiometry the BVS for the 12-coordinate Sr^{2+} cation is estimated to be 1.75.

At temperatures of 370 K and above superlattice reflections indicative of out-of-phase octahedral tilting were no longer observed in the neutron diffraction profiles (Fig. 3), although the broad weak features near $2\theta=138°$ and 146° (and elsewhere in the pattern), which can be indexed as *M* point superlattice reflections, suggest that the in-phase tilts persisted to 380 K. No systematic variation in displacement parameters of the anions was observed. The weakness of these additional reflections meant that it was possible to obtain a satisfactory refinement to a cubic model in $Pm\bar{3}m$, although this cubic model did not account for these additional weak reflections observed in the pattern obtained at 380 K. It appears that an additional phase exists between the orthorhombic and cubic phases, albeit over a very narrow temperature range.

By comparison with other $SrMO_3$ perovskites a direct orthorhombic to cubic transition in $Sr_{0.92}NbO_3$ is unlikely. In the chemically closely related $SrZrO_3$ [4], $SrMoO_3$ [8], $SrRuO_3$ [5] and $SrSnO_3$ [6] systems the *R* point mode softens well before the *M* point mode, resulting in the formation of an intermediate tetragonal phase in *I*4/*mcm*. The neutron diffraction patterns of tetragonal $SrZrO_3$ [1,4] and $SrMoO_3$ [8] contain moderately strong and well resolved *R* point superlattice reflections. Secondly a direct transition implies a softening of the entire Brillouin branch from the *R* point to the *M* point at the transition temperature. Such a softening is rarely observed, although it has been proposed that it occurs in neighbourite ($NaMgF_3$) as a consequence of strong coupling between the in-phase and out-of-phase tilts [4]. Doping $NaMgF_3$ with K apparently modifies this coupling and an intermediate tetragonal phase in *P*4/*mbm* ($a^0a^0c^+$) is described in solid solutions of the type $Na_{1-x}K_xMgF_3$ [25]. The diffraction pattern of perovskites in *P*4/*mbm* will display *M* point reflections indicative of in-phase tilts of the octahedra in addition to the parent Bragg reflections. Although weak, such peaks are present in the neutron diffraction patterns.

It is possible to separate the primary order parameters, and their temperature variation, from other spontaneous structural distortions present in the distorted phases by symmetry-mode decomposition of the observed structural distortion. Both the primary and secondary distortion components in perovskites can be quantitatively resolved by a full symmetry-mode decomposition of the distortion as has been shown by Knight [26] in the halo-perovskite $KCaF_3$. This has the major advantage that it allows the distortions of the octahedra to be separated from the cooperative tilting [26–28]. For a review on the symmetry-mode analysis of distorted structures see [29].

To better understand the nature of the transition to the cubic structure the amplitudes of the distortion modes in the orthorhombic phase of $Sr_{0.92}NbO_3$ were estimated from the refined structures using the program AMPLIMODES [30] and the temperature dependences of these are presented in Fig. 4. Five primary modes are present in the *Pnma* structure, two of which, M_{3^+} and R_{4^+}, are associated with the in-phase and out-of-phase tilts of the octahedra. Here we are describing the cubic perovskite such that the oxygens occupy the 1*d* Wyckoff sites. The $X_{5^+}(O)$, $R_{5^+}(O)$ and M_{2^+} modes describe deformation of the NbO_6 octahedra whilst the $X_{5^+}(Sr)$ and $R_{5^+}(Sr)$ modes also have a contribution associated with displacement of the *A*-type Sr cation [29]. As is evident from Fig. 4 the M_{3^+} and R_{4^+} modes are strongly temperature dependent, whereas those of the remaining modes are much smaller and they do not exhibit any systematic dependence on temperature.

The M_{3^+} mode is the stronger of the two tilting modes and this apparently persists to a slightly higher temperature than the R_{4^+} mode. By comparison in $SrZrO_3$ the R_{4^+} mode is the dominant mode and this persists to higher temperatures, resulting in observation of the *Imma* and *I*4/*mcm* space groups [4]. The

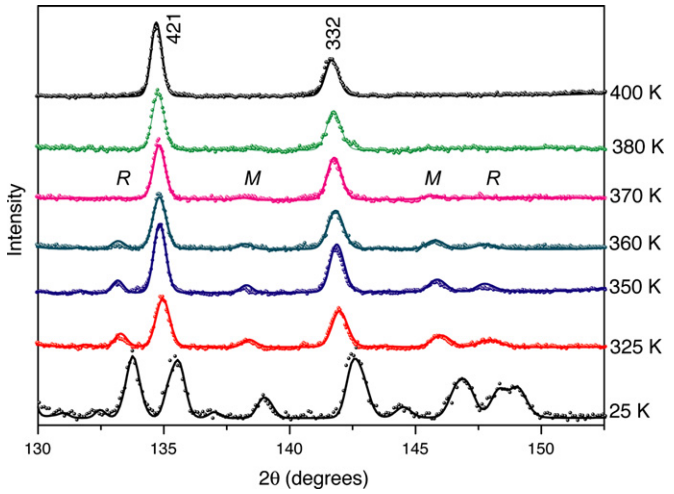

Fig. 3. Selected region of the powder neutron diffraction patterns for $Sr_{0.92}NbO_3$. The solid lines are the results of the Rietveld fitting to the patterns. Note the persistence of the *M* point superlattice reflections indicative of in-phase titling of the NbO_6 octahedra in the profiles at 370 and 380 K.

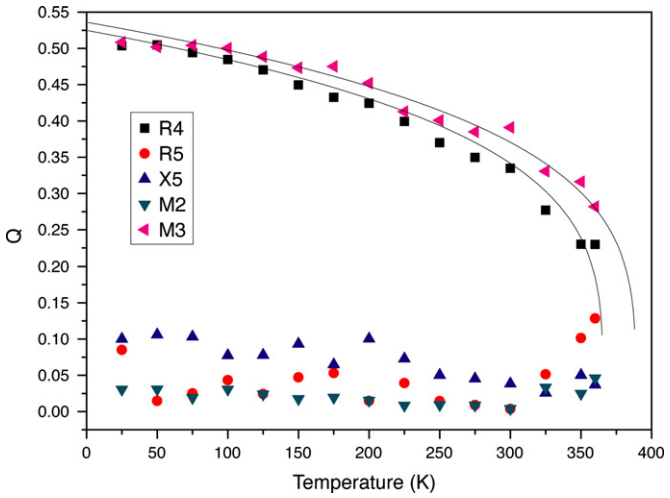

Fig. 4. Temperature dependence of amplitude (*Q*) of the various modes present in the *Pnma* structure of $Sr_{0.92}NbO_3$. The M_3 mode is seen to persist to higher temperature than the R_4 mode suggesting the out-of-phase tilts are lost before the in-phase tilts and that a phase intermediate between *Pnma* and $Pm\bar{3}m$ exists.

temperature dependence of the M_{3+} and R_{4+} modes can be treated as an order parameter for the phase transition and both exhibit a Q^4 type temperature dependence and suggest transition temperatures of 365 and 388 K, Fig. 4. Examination of the neutron profiles shown in Fig. 3 shows that the intensity at the *R* point reflections is absent in the patterns recorded at or above 370 K but, as noted above, there is an indication of a small amount of residual intensity of the *M* point reflection near $2\theta \sim 138^\circ$ and 146° present in the patterns recorded at 370 and 380 K Fig. 3. This suggests that, as was observed in $Na_{1-x}Sr_xNbO_3$, a *P*4/*mbm* phase exists intermediate between the *Pnma* and $Pm\bar{3}m$ phases in $Sr_{0.92}NbO_3$ [23]. It was possible to fit the neutron profiles obtained at 370 and 380 K to a model in *P*4/*mbm* and the results of this fitting are summarised in Table 1. Evidently the sequence of transitions is $Pnma \rightarrow P4/mbm \rightarrow Pm\bar{3}m$. Group theory demonstrates that both transitions are allowed to be continuous [31] and the progressive decrease in intensity of the various superlattice reflections on heating is consistent with this.

Given the noise in the secondary distortions there is some merit in using higher quality neutron diffraction data to directly refine the amplitudes of the symmetry-adapted basis modes describing static structural distortions rather than the individual atomic positions. Although beyond the scope of the present study such work would establish what, if any, systematic variations in the weak distortions associated to secondary modes exist [29].

The temperature dependences of the lattice parameters and cell volume are illustrated in Figs. 5 and 6. There is a clear change in the rate of thermal expansion of the cell volume associated with the transition to the cubic structure. The volume of the appropriately scaled orthorhombic phase is somewhat less that that estimated by extrapolation of the high temperature cubic volumes. Such behaviour has been observed in numerous other perovskites where the onset of tilting is accompanied by a small volume reduction. Despite the occurrence of the two phase transitions over a narrow temperature range, there is no evidence to suggest there is a discontinuous change in volume.

There is a dramatic reduction of the average Nb–O distance associated with the transition to the cubic structure transition as illustrated in Fig. 7. This is similar to that seen for $NaMgF_3$ [25] but is different from that observed for $SrZrO_3$. In the orthorhombic phase the tilting of the octahedra acts to increase the average Nb–O distance. Heating the sample increases the cell volume but reduces the magnitude of the tilting and the sum of these effects is apparent in the reduction of the average Nb–O bond distance. This is presumably necessary to maintain a favourable bond valence of the cations as required by Brown's [32] distortion

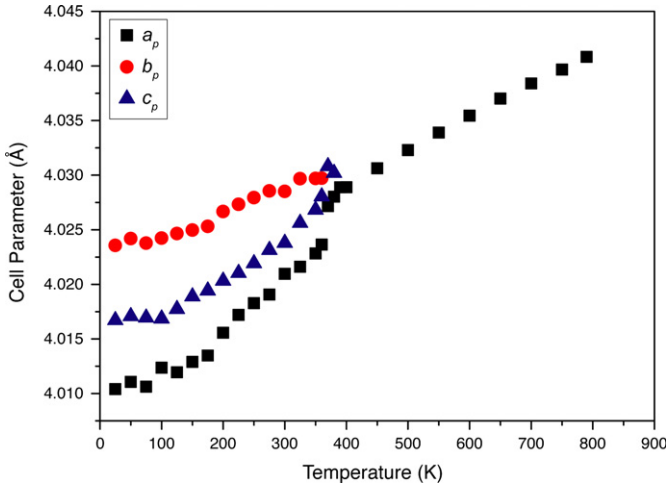

Fig. 5. Temperature dependence of the equivalent primitive unit cell parameters for $Sr_{0.92}NbO_3$. Below 360 K the parameters are for refinements in *Pnma* and above 390 K they are for refinement in $Pm\bar{3}m$. The structure at 370 and 380 K was refined in *P*4/*mbm*.

Table 1
Crystal data and selected details for the structural refinements of $Sr_{0.92}NbO_3$ based on neutron diffraction data.

Temperature (K)	25	350	370	390
Space group	*Pnma*	*Pnma*	*P*4/*mbm*	$Pm\bar{3}m$
a (Å)	5.6720(4)	5.6891(2)	5.69526(22)	4.02853(3)
b (Å)	8.0479(3)	8.0594(1)	$=a$	$=a$
c (Å)	5.6808(3)	5.6948(1)	4.03082(33)	$=a$
Volume (Å^3)	259.31(3)	261.110(9)	130.655(19)	65.3820(9)
Sr *x*	0.0084(26)	0.0010(20)	0	½
Sr *y*	1/4	1/4	1/2	1/2
Sr *z*	0.5059(46)	0.5002(69)	1/2	1/2
Sr B_{iso}	0.37(7)	1.22(4)	1.10(4)	1.70(2)
Nb B_{iso} (Å^2)[a]	0.05(4)	0.23(3)	0.64(4)	0.74(2)
O1 *x*	0.4975(34)	0.4957(22)	0	1/2
O1 *y*	1/4	1/4	0	0
O1 *z*	0.4701(18)	0.4920(46)	1/2	0
O1 B_{iso} (Å^2)	0.27(16)	0.61(11)	1.45(4)[b]	1.37(7)[c]
O2 *x*	0.2287(14)	0.2371(11)	0.2566(6)	
O2 *y*	−0.0166(7)	−0.0104(6)	0.7566(6)	
O2 *z*	0.2738(15)	0.2651(10)	0	
O2 B_{iso} (Å^2)	0.24(8)	1.17(6)	0.93(3)	
Nb–O1 (Å)	2.0192(9) × 2	2.0155(6) × 2	2.0154(2) × 2	2.01427(1) × 6
Nb–O2 (Å)	2.030(11) × 2	2.026(8) × 2	2.0143(1) × 4	
Nb–O2 (Å)	2.009(11) × 2	2.008(8) × 2		
R_p (profile) (%)	9.27	7.15	7.55	7.30
R_{wp} (weighted profile) (%)	8.55	9.95	10.06	9.39

[a] In all cases Nb is at the origin (0 0 0) of the cell.
[b] Refined anisotropic O(1): $U^{11}=U^{22}=3.2(7)\times 100$ Å^3, $U^{33}=0.5(4)\times 100$ Å^3; O(2): $U^{11}=4.6(4)\times 100$ Å^3, $U^{22}=0.2(4)\times 100$ Å^3, $U^{33}=2.3(2)\times 100$ Å^3, $U^{12}=0.5(4)\times 100$ Å^3.
[c] Refined anisotropic $U^{11}=U^{22}=1.46(6)\times 100$ Å^3, $U^{33}=4.12(16)\times 100$ Å^3.

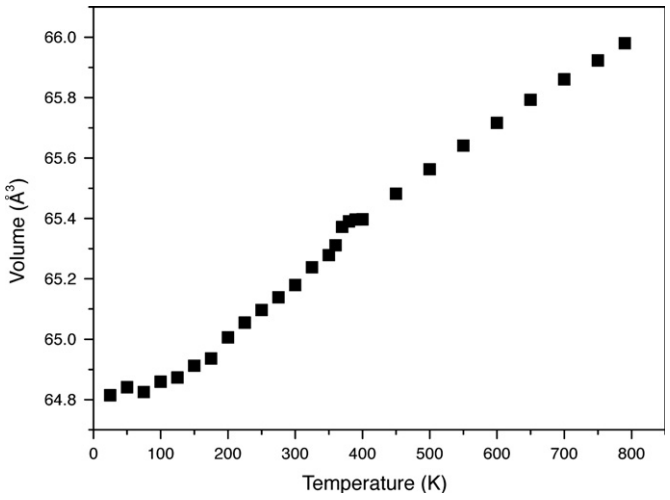

Fig. 6. Temperature dependence of the appropriately scaled unit cell volume for $Sr_{0.92}NbO_3$, illustrating an apparent discontinuity near 370 K.

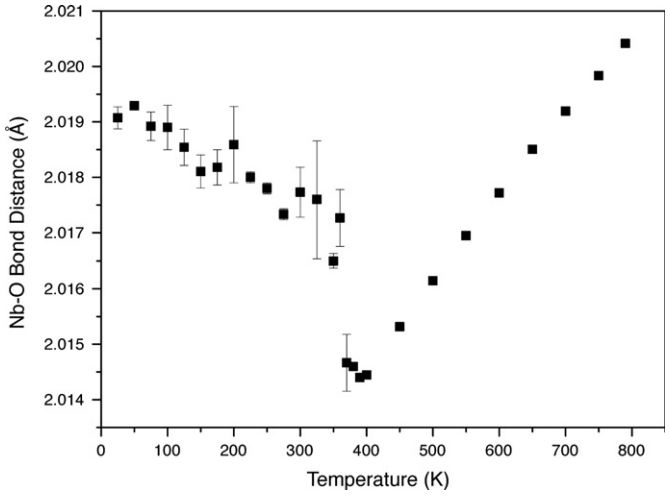

Fig. 7. Temperature dependence of mean Nb–O bond distances in $Sr_{0.92}NbO_3$ derived from Rietveld refinements of the neutron diffraction data. Notice the dramatic shortening of Nb–O distance accompanying the transition from the orthorhombic structure.

theorem. The rapid decrease in the average Nb–O distance reflects the fact that the in-phase and out-of-phase tilts vanish over a relatively narrow temperature range. Once the cubic structure is obtained the observed systematic increase in the bond distances reflects the thermal expansion of the unit cell.

In summary $Sr_{0.92}NbO_3$ displays a different sequence of structures on heating, namely $Pnma \rightarrow P4/mbm \rightarrow Pm\bar{3}m$, from that observed for other second row perovskites $SrMO_3$ (M=Zr, Mo, Ru and Rh). The reason for this is not immediately apparent. The size of the transition metal cations decreases from Zr to Rh, [22], with a concurrent increase in the tolerance factor so that the cubic structure should be observed at progressively lower temperatures. As summarised in Table 2 this is not observed, suggesting that the *d*-electron configuration does impact the stability of the various structures. The importance of the *d* electrons is clearly evident in the simple dioxides MO_2, where ZrO_2 has a unique (for the current series) structure, NbO_2 [33], MoO_2 [34] and TcO_2 [35] adopt distorted rutile-type structures as a consequence of metal–metal bonding, and RuO_2 and RhO_2 adopt a regular rutile-type structure [36,37]. Heating NbO_2 results in a transition to a regular rutile structure, but even so the structure

Table 2
Selected structural and spectroscopic data for some $SrMO_3$ perovskites.

Cation	Ionic radii (Å)[a]	Tolerance factor	d^n	T_{cubic} (K)	Δ (eV)[b]	Reference
Zr	0.72	0.947	0	1360	7.5	[31]
Nb	0.68	0.965	1	388	–	This work
Mo	0.65	0.980	2	266	3.5	[8]
Tc	0.645	0.982	3	>300	–	[38]
Ru	0.620	0.994	4	945	3.3	[5]
Rh	0.60	1.004	5	>1073	2.5	[7]

T_{cubic} is the temperate at which the structure transforms from tetragonal to cubic.

[a] From [22].
[b] From [39,40].

shows subtle distortion of the NbO_6 octahedra, reflecting the presence of *d*-electron configuration [33]. In going across this series the number of *d* electrons and the magnitude of the splitting of the *d*-orbitals change. $SrZrO_3$ is a $4d^0$ insulator in which the Zr 4*d* band, which is split into t_{2g} and e_g bands (using octahedral notation), is the lowest unfilled level. In $SrNbO_3$ the single *d* electron will occupy the t_{2g} band and $SrNbO_3$, like $SrMoO_3$, is a Pauli paramagnetic band metal. In $SrRuO_3$ the d^4 electrons all occupy the t_{2g} band and this is an example of a ferromagnetic metal whilst $SrRhO_3$ is also low spin and is a d^5 paramagnetic metal. Little is known about $SrTcO_3$, although we have established that this is orthorhombic in *Pbnm* at room temperature [38]. It is possible that variation in T_{cubic} is a consequence of the hybridisation of the *M* 4*d* and O 2*p* orbitals and *M*–O π-bonding. O 1*s* X-ray absorption spectroscopy of the four $SrMO_3$ oxides (M=Zr, Mo, Ru and Rh) suggests there is a non-linear decrease in hybridisation strength as the number of 4*d* electrons increases, which reflects the decreasing size of the 4*d* orbitals [39,40]. The importance of *M*–O π-bonding is most evident from the change in T_{cubic} in going from Zr (d^0) to Nb (d^1) and in Mo (d^2) to T_{cubic} (d^3). In $SrTcO_3$ the t_{2g} orbitals are all singularly occupied. Evidently it is possible to rationalise the initial decrease in T_{cubic} for the d^0–d^2 and subsequent increase for d^3–d^5 based on competing effects of size and *M*–O π-bonding. However, further studies are needed to understand why softening of the Brillouin zone at the *M* point is favoured for $SrNbO_3$ but for all other $SrMO_3$ oxides where *M* is a 4*d* metal softening occurs at the *R* point.

4. Conclusion

The temperature dependence of the structure of $Sr_{0.92}NbO_3$ was investigated between 25 and 700 K. Unlike the other well studied 4*d* Sr perovskites $SrMO_3$ (M=Zr, Mo, Ru and Rh) the transition to the cubic phase involves the sequence $Pnma \rightarrow P4/mbm \rightarrow Pm\bar{3}m$. It is proposed that the unanticipated softening of the *M* point is a consequence of competition between size and π-bonding effects.

Acknowledgment

B.J.K. acknowledges the support of the Australian Research Council for this work.

References

[1] B.J. Kennedy, C.J. Howard, B.C. Chakoumakos, Phys. Rev. B. 59 (1999) 4023–4027.
[2] M. Ahtee, A.M. Glazer, A.W. Hewat, Acta Crystallogr. Sect. B 34 (1978) 752–758.
[3] L. Carlsson, Acta Crystallogr. 23 (1967) 901 &.

[4] C.J. Howard, K.S. Knight, B.J. Kennedy, E.H. Kisi, J. Phys.: Condens. Matter 12 (2000) L677–L683.
[5] B.J. Kennedy, B.A. Hunter, J.R. Hester, Phys. Rev. B 65 (2002) 2241031–2241034.
[6] M. Glerup, K.S. Knight, F.W. Poulsen, Mater. Res. Bull. 40 (2005) 507–520.
[7] B.J. Kennedy, K. Yamaura, E. Takayama-Muromachi, J. Phys. Chem. Solids 65 (2004) 1065–1069.
[8] R.B. Macquart, B.J. Kennedy, M. Avdeev, J. Solid State Chem. 183 (2010) 250–255.
[9] D. Ridgley, R. Ward, J. Am. Chem. Soc. 77 (1955) 6132–6136.
[10] H. Hannerz, G. Svensson, S.Y. Istomin, O.G. D'Yachenko, J. Solid State Chem. 147 (1999) 421–428.
[11] N.H. Peng, J.T.S. Irvine, A.G. Fitzgerald, J. Mater. Chem. 8 (1998) 1033–1038.
[12] K. Isawa, J. Sugiyama, K. Matsuura, A. Nozaki, H. Yamauchi, Phys. Rev. B 47 (1993) 2849–2853.
[13] S.Y. Istomin, G. Svensson, J. Kohler, J. Solid State Chem. 167 (2002) 7–16.
[14] B.J. Kennedy, B.A. Hunter, Phys. Rev. B 58 (1998) 653–658.
[15] B.J. Kennedy, A.K. Prodjosantoso, C.J. Howard, J. Phys.: Condens. Matter 11 (1999) 6319–6327.
[16] R.E.A. McKnight, C.J. Howard, M.A. Carpenter, J. Phys.: Condens. Matter 21 (2009) 14.
[17] P.J. Saines, B.J. Kennedy, R.I. Smith, Mater. Res. Bull. 44 (2009) 874–879.
[18] K.D. Liss, B. Hunter, M. Hagen, T. Noakes, S. Kennedy, Physica B 385-386 (2006) 1010–1012.
[19] K.S. Wallwork, B.J. Kennedy, D. Wang, AIP Conf. Proc. 879 (2007) 879–882.
[20] B.A. Hunter, C.J. Howard, in: A Computer Program for Rietveld Analysis of X-Ray and Neutron Powder Diffraction Patterns, Lucas Heights Research Laboratories, Sydney, 1998, pp. 1–27.
[21] B.J. Kennedy, C.J. Howard, B.C. Chakoumakos, J. Phys.: Condens. Matter 11 (1999) 1479–1488.
[22] R.D. Shannon, Acta Crystallogr. Sect. A 32 (1976) 751–767.
[23] S.Y. Istomin, G. Svensson, O.G. D'Yachenko, W. Holm, E.V. Antipov, J. Solid State Chem. 141 (1998) 514–521.
[24] M.T. Casais, J.A. Alonso, I. Rasines, M.A. Hidalgo, Mater. Res. Bull. 30 (1995) 201–208.
[25] Y.S. Zhao, J. Solid State Chem. 141 (1998) 121–132.
[26] K.S. Knight, Can. Mineral. 47 (2009) 381–400.
[27] C.N.W. Darlington, Acta Crystallogr. Sect. A 58 (2002) 66–71.
[28] C.N.W. Darlington, Acta Crystallogr. Sect. A 58 (2002) 299–300.
[29] J.M. Perez-Mato, D. Orobengoa, M.I. Aroyo, Acta Cryst. A66 (2010) 558–590. doi:10.1107/S0108767310016247.
[30] D. Orobengoa, C. Capillas, M.I. Aroyo, J.M. Perez-Mato, J. Appl. Cryst. 42 (2009) 820–833.
[31] C.J. Howard, H.T. Stokes, Acta Crystallogr. Sect. B 54 (1998) 782–789.
[32] I.D. Brown, Struct. Bonding 2 (1981).
[33] A.A. Bolzan, C. Fong, B.J. Kennedy, C.J. Howard, J. Solid State Chem. 113 (1994) 9–14.
[34] A.A. Bolzan, B.J. Kennedy, C.J. Howard, Aust. J. Chem. 48 (1995) 1473–1477.
[35] E.E. Rodriguez, F. Poineau, A. Llobet, A.P. Sattelberger, J. Bhattacharjee, U.V. Waghmare, T. Hartmann, A.K. Cheetham, J. Am. Chem. Soc. 129 (2007) 10244–10248.
[36] A.A. Bolzan, C. Fong, B.J. Kennedy, C.J. Howard, Acta Crystallogr. Sect. B 53 (1997) 373–380.
[37] D.P. Romanov, V.N. Skrobot, Glass Phys. Chem. 35 (2009) 518–524.
[38] M.L. Carter, G.J. Thorogood, B.J. Kennedy, in preparation.
[39] Y.S. Lee, J.S. Lee, T.W. Noh, D.Y. Byun, K.S. Yoo, K. Yamaura, E. Takayama-Muromachi, Phys. Rev. B 67 (2003) 113101.
[40] H.J. Noh, B.J. Kim, S.J. Oh, J.H. Park, H.J. Lin, C.T. Chen, Y.S. Lee, K. Yamaura, E. Takayama-Muromachi, J. Phys.: Condens. Matter 20 (2008) 5.